Laminar-flow design for a Mach-6 quiet-flow wind tunnel nozzle

Steven P. Schneider

School of Aeronautics and Astronautics, Purdue University, West Lafayette, IN 47907-1282, USA

A high Reynolds-number Mach-6 wind-tunnel nozzle has been designed for a new quiet-flow Ludwieg tube. The quiet-flow nozzle is designed to maintain laminar boundary layers on the nozzle walls as far downstream as possible. Transition onset is estimated using the e^N method. A very long nozzle with gentle curvature is used to reduce Görtler instability. Early transition would occur in adiabatic nozzles of this type, due to the first-mode TS instability. The first mode is controlled with an isothermal wall temperature that is high near the throat and tapers to ambient near the exit. The crossflow instability is eliminated through use of an axisymmetric nozzle. The e^N method predicts that a quiet-flow Reynolds number in excess of 13 million can be achieved in a prototype nozzle that is 2.61 m (103 inch) long and 0.23 m (9 inch) in diameter, at 10 atm. (1.03×10^6 Pa) total pressure. This performance would be about twice that of the existing Langley Mach-6 quiet-flow nozzle. At the same pressure, a nozzle that is 10 m (33 ft) long and 0.61 m (24 in.) in diameter is predicted to have a quiet Reynolds number of more than 36 million, a value sufficient to allow reproducing many flight experiments.

LAMINAR-turbulent transition in high-speed boundary layers is important for prediction and control of heat transfer, skin friction, and other boundary layer properties. However, the mechanisms leading to transition are still poorly understood, even in low-noise environments. Applications hindered by this lack of understanding include reusable launch vehicles such as the X-33 (ref. 1), high-speed interceptor missiles[2] and hypersonic cruise vehicles[3].

The transition process is initiated through the growth and development of disturbances originating on the body or in the freestream[4]. These disturbances generate instability waves which grow and break down into turbulence[5–10]. The best commonly-available design tool uses correlations between transition and the integrated growth of the linear instability waves[5]. Although these e^N correlations neglect all receptivity, nonlinear, and secondary instability effects, they work fairly well for a variety of conditions where the environmental noise is generally low[11,12].

Unambiguous progress in characterizing the mechanisms of low-speed transition has been made through the use of low-noise wind tunnels with disturbance levels comparable to those in flight, and the study of the development of controlled perturbations. In contrast, the interpretation of most high-speed experiments has been ambiguous due in part to operation in high-noise wind tunnels with disturbance levels much larger than those in flight. Only in the last two decades have low-noise supersonic wind tunnels been developed[13,14]. This development has been difficult, since the boundary layers on the nozzle walls must be kept laminar in order to avoid high levels of eddy-Mach-wave acoustic radiation from the normally-present turbulent boundary layers. The effects of this acoustic noise are profound. For example, linear instability theory suggests that the transition Reynolds number on a 5 degree half-angle cone should be 0.7 of that on a flat plate, but noisy tunnel data showed that the cone transition Reynolds number was actually higher than the flat plate result. Only when quiet tunnel results were obtained was the theory verified[15]. Consequently, both the location and the parametric trends for transition in conventional wind tunnels can be dramatically different from those in flight[12]. Only the study of controlled disturbances in a controlled quiet environment can produce unambiguous data suitable for development of reliable theory. Reliable predictive methods will have to be based on estimates of the flight disturbance environment.

To address hypersonic transition applications, NASA Langley constructed a Mach-6 quiet tunnel[16]. This tunnel was designed using e^N methods, and the performance agreed fairly well with an $N = 7.5$ criterion. A number of experiments were carried out in this facility before it was deactivated[17]. A Mach-8 quiet tunnel has also been under development at Langley[14].

The present work is part of a program to develop an improved hypersonic quiet tunnel with low operating costs[18,19]. The Mach number was chosen to be 6, which is near the lowest Mach number at which the hypersonic

e-mail: steves@ecn.purdue.edu

Satish Dhawan played a major role in leading study of laminar–turbulent transition from empirical correlations toward a scientific understanding based on the physical mechanisms. The work described here continues a 30-year experimental effort toward this same goal and has drawn inspiration from Prof. Dhawan and the other early leaders.

second-mode instability is dominant under coldwall conditions[20]. The hypersonic insensitivity of transition to roughness can also be studied at Mach 6 (ref. 21). The limited temperatures required to reach Mach 6 reduce construction, operating, and instrumentation costs.

Design methods

The methods used for design of the quiet-flow nozzles are very nearly the same ones used by NASA Langley for its designs[22]. The major difference from the Langley methods is that the supersonic uniform-flow-exit nozzle shape is computed using the wind-tunnel nozzle design code used for the AEDC tunnels[23,24], instead of a Langley-modified form of the short-rocket-nozzle code of Nelms[25]. The Sivells code used already included the ability to create radial-flow sections between the initial expansion contour and the latter part of the contour (which cancels the characteristics in order to provide uniform flow at the exit)[23]. Harris's boundary-layer code is used for the laminar boundary-layer[26]. The e**Malik code is used for the e^N stability computations[27,28]. The number of circumferential waves is held constant in the Görtler computation[22]. The present author was able to repeat earlier computations of the N-factor for Görtler instability on the wall of the Langley Mach-6 quiet nozzle[29].

The input/output of the three codes has been modified by the author, to create an automatic system that feeds the output of one code into the input of the next, with minimal user labour[29]. The bleed slot lip ahead of the throat is computed using the Hopkins-Hill technique, just as it has been at Langley, except a new, documented version was written[30]. The suction side of the bleed slot lip has been designed by the method of streamtubes[31]. The design of the contraction and bleed-slot area is described together with the mechanical design in ref. 32.

Excellent resolution in the boundary-layer and instability analyses is necessary to achieve accurate stability results[33]. Extensive grid-resolution tests were therefore carried out. In the boundary-layer code, 201 points were used in the wall-normal direction, although a comparison between most-amplified Görtler N factors from computations with 201 and 101 points yielded a difference of only 0.3% at the nozzle exit. In the Harris boundary layer code, the geometrical progression factor xk was taken as 1.05 to 1.10, for a fairly uniform grid with a small amount of packing near the wall. This is because good accuracy near the boundary-layer edge is needed. The boundary layer profiles were obtained to about 1.25 times the 99.99% boundary-layer edge thickness, to make sure that the derivatives near the boundary layer edge were fully resolved. This was a very conservative grid, since a comparison to a grid with 1/3 fewer points near the boundary-layer edge yielded a difference in second-mode N-factor of less than 0.2% at the nozzle exit.

The first derivatives of the velocity and temperature profiles are written directly from the Harris code, so only one numerical differentiation is required to generate second derivatives for input to e**Malik. Figures 25–27 in ref. 34 show that changing the streamwise resolution from 254 profiles to 398 profiles changed the most-amplified N-factor by less than 1%. The streamwise resolution given is the number of stations computed in the e**Malik code; the number of streamwise boundary-layer solution stations was twice this. In e**Malik, 141 grid points were used in each local eigenvalue search, a number near the maximum allowable, again to be conservative. The major difficulty was obtaining accurate streamwise radii of curvature for the Görtler analysis; this was surmounted by writing the first and second derivatives of the streamwise wall contour directly from where they are computed inside the Sivells code. The integrated N-factors are thus thought to be accurate to about 1%. Further details are contained in ref. 34.

Approach

Lengthen the nozzle to achieve higher quiet-flow Reynolds numbers

Ref. 35 shows experimental data to demonstrate that lengthening a nozzle extends the quiet-flow Reynolds number. This concept is discussed in some detail with respect to another Langley Mach-2.4 design[36], which provides e^N computations. Figures 1 and 2 in ref. 36 show that a nozzle that is 3 times larger when operated at 1/3 of the total pressure yields nearly identical quiet-flow length Reynolds number, with transition occurring in nearly the same relative location for the two nozzles. This scaling indicates that Görtler-induced transition also scales with Reynolds number, as will be discussed further later. Ref. 36 also showed that a nozzle of approximately twice the length increased the quiet-flow length Reynolds number ($R_{\Delta x}$) by a factor of about two.

Heat the nozzle throat to delay transition

A further transition delay might be expected if the nozzle throat is heated[37]. Ref. 38 explains the likely mechanism – note that although this second reference is for incompressible flow, the trend with wall cooling is the same for first-mode compressible waves, which may be a major factor in the first part of the nozzle. Although the effect of heating on the Görtler instability may be small, the heating will also thicken the throat-region boundary layer and so reduce the relative roughness height. Langley observations indicate that a hot nozzle can increase the extent of quiet flow[39]. These results were confirmed indirectly by measurements in the Purdue tunnel carried out with hot driver-tube gas

(to which the wall appears cold); these results show a decrease in quiet-flow Reynolds number[40].

Reference 41 discusses the favourable effect of throat heating, but raises a new concern about a second generalized inflection point that can arise in the throat area when large amounts of heating are used. In the present case, the peak throat temperature is limited to values that are low by the standards of ref. 41, because of the limitations of cost-effective nozzle materials. No evidence of a second generalized inflection point is seen in plots similar to Figure 3 of ref. 41.

Results

Nozzle shapes

Figure 1 shows the inviscid contours of three nozzles designed with Sivell's code[24]. Choices had to be made in setting the input parameters for this code. A 3rd-degree axial velocity distribution was chosen in the throat region, and a 4th-degree velocity distribution was chosen in the exit region. Neither of these selections is thought to be critical. The contour of the Langley Mach-6 quiet tunnel is also shown – this contour includes the displacement thickness correlation. Some key parameters are shown in Table 1. Here, ID is the case number for the nozzle; each nozzle was assigned a letter identifying the inviscid design, followed by a number identifying the viscous conditions. These IDs will be shown in parentheses in the plots. All lengths are given in throat radii, and the coordinate origin is on the centerline at the throat. The nozzles were scaled geometrically to various sizes. Nozzle m6chen6 is very similar to the Langley Mach-6 design, although the similarity is obscured somewhat in this plot since the Langley exit diameter is 0.19 m (7.5 in.). The long nozzle, *g*, has half the inflection-point angle and about twice the length. The very long nozzle, *i*, has an inflection angle which is halved again. The 4th nozzle, *m*, was shortened because the additional length is not needed for the prototype. The 5th nozzle, *l*, is the same as *i*, except it was computed with higher resolution. The length of the radial flow region generally increases with nozzle length.

Further validation

Computations were carried out for the nozzle similar to that used at NASA Langley. Envelopes of the first-mode and Görtler instabilities were computed[34]. The results are similar to those reported by Chen[22]; Görtler instability dominates. The nozzle wall was adiabatic, $T_t = 456$ K (820 R), and the inviscid exit diameter (without the displacement thickness correction) is 0.20 m (8.0 in.).

Figure 2 shows the quiet-flow length Reynolds number for the shorter nozzles, computed and compared to results for the Langley Mach 6. The Langley data were digitized from figure 9 in ref. 42. Of course, there are many uncertainties in a semi-empirical prediction method of this type; these uncertainties include nonlinear effects in the growth of individual instabilities, nonlinear effects in the combined effects of several instabilities, and receptivity effects. Computations using the Parabolized Stability Equations (PSE) would have been useful, because they could include nonparallel,

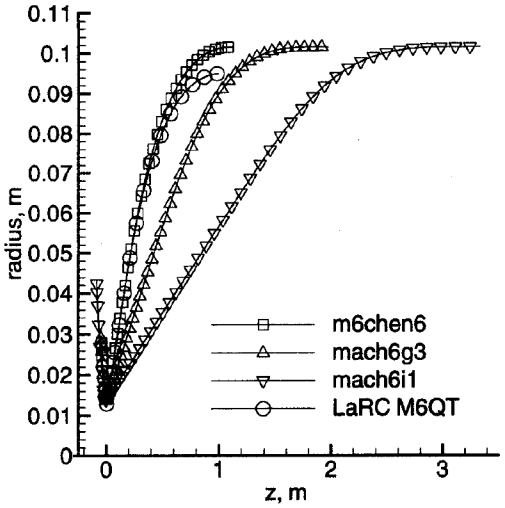

Figure 1. Inviscid contours for 3 axisymmetric nozzles with 0.20 m (8 in.) exits.

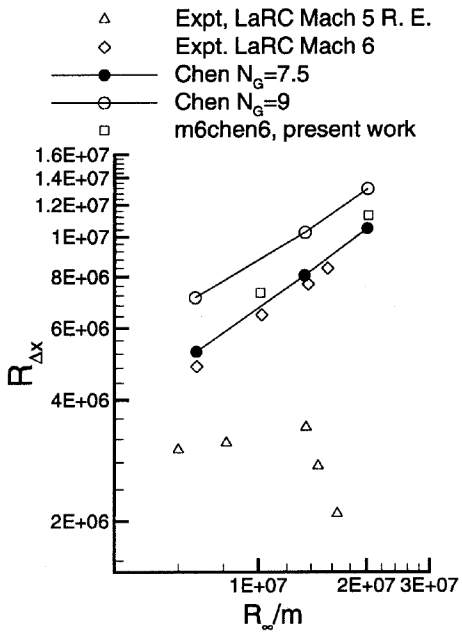

Figure 2. Quiet Reynolds numbers for Langley and Langley-like nozzles (m6chen6b, m6chen6c).

Table 1. Key parameters for inviscid nozzle designs

ID	η	RC	x_g	y_g	x_a	y_a	x_d	y_d
m6chen6	9.84	3.68	3.39	1.50	12.82	3.13	81.85	7.29
g	4.92	4.00	1.81	1.13	28.42	3.42	142.1	7.29
i	2.46	8.00	1.43	1.05	72.32	4.09	240.7	7.29
m	4.00	8.00	2.13	1.12	38.31	3.65	164.9	7.29
l	2.46	8.00	1.43	1.05	72.32	4.09	240.7	7.29

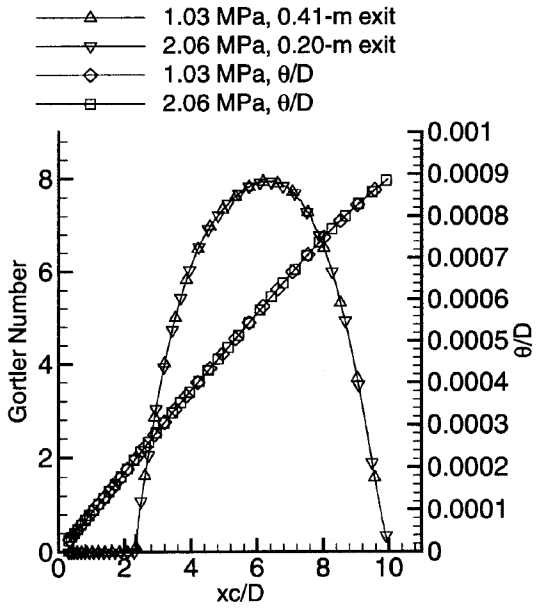

Figure 3. Görtler number for two long Mach-6 nozzles with different scalings (g5, g6).

non-linear, and wave interaction effects that are neglected in the present analysis. However, use of the particular PSE methods that were available at the time was considered to be beyond the scope of this effort.

Earlier predictions by Chen[42] agreed well with data in the Langley quiet nozzles when an *N*-factor of 7.5 was used as a transition criterion. Chen used $N = 7.5$ based on only the most amplified instability; the second-mode instability was not computed, and since the *N*-factor for the first mode was 2 or 3 it was also neglected[22]. Since the various instability-wave types have varying relative sizes in the computations presented here, some method of accounting for their overall effect on transition is needed. Unfortunately, there is little data for nonlinear growth and interaction effects. Here, transition will be based on the 'combined *N*-factor', N_{tot}, which is the square root of the sum of the squares of the individual *N* factors. This simple estimate is without theoretical or empirical justification, except that it is similar to one used successfully by Schrauf for crossflow and TS instability on swept wings[43]. Predictions will be based primarily on $N_{tot} = 7.5$, which is more conservative than Chen's method since it includes the effect of the smaller instabilities.

Using this method, transition was predicted on the nozzle walls, and the characteristic lines from the inviscid nozzle solution were used to predict the extent of quiet flow. The results for $N = 7.5$ are very similar to Chen's results, and to the original data from the Mach-6 quiet tunnel. The new nozzle performs a bit better, for Figure 2 shows that $R_{\Delta x}$ is higher even though the TS *N*-factor is included in our prediction method. The slope is about the same; the quiet Reynolds number increases with nozzle Reynolds number.

Scaling

Figure 3 shows results computed in the long nozzle at the same nozzle Reynolds number, to determine Reynolds number effects. The two cases achieve Reynolds number by a different combination of size and pressure. When scaled with Reynolds number and exit diameter, the results for the momentum thickness and Görtler number are identical. Obviously, Görtler number scales with size and Reynolds number. The stagnation temperature is 456 K (820 R), and the stagnation pressure and nozzle exit diameter are shown in the legend. The nozzle wall is isothermal for these computations, with an inlet temperature equal to the stagnation temperature, and a wall temperature that tapers linearly to 300 K (540 R). This temperature distribution is similar to that which is expected in the tunnel – the driver tube must be continuously maintained at stagnation temperature for Mach 6, and it will heat the upstream end of the nozzle by conduction. The downstream end will be cold due to conduction to the piping.

Figure 4 shows *N*-factor results for the same two cases. The envelope of the most amplified first-mode and Görtler waves is plotted, for each nozzle. The horizontal axis is the arclength along the nozzle wall scaled with the nozzle exit diameter. The curves overlap to within 1 per cent. Thus, the instability computations scale with diameter and Reynolds number, even though the frequencies and Görtler wave number differ by a factor of 2. Reynolds number can be achieved with size or pressure, and the e^N results are identical in either case. This plot serves to validate the computational methods as well as the scaling.

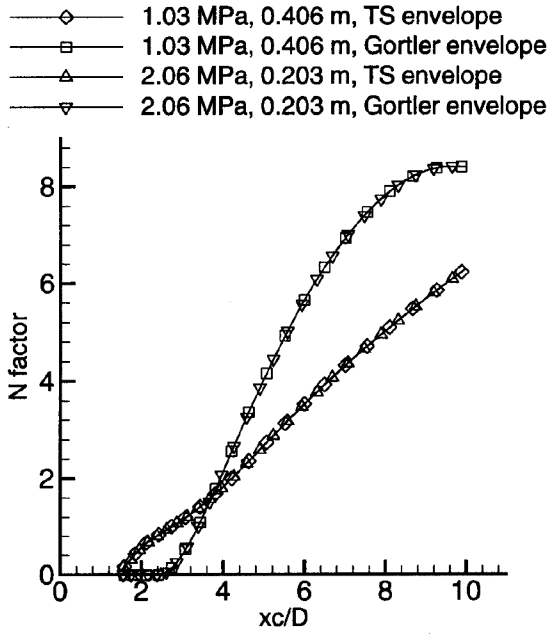

Figure 4. TS and Görtler envelopes for two nozzles at different scales but the same Reynolds number (g5, g6).

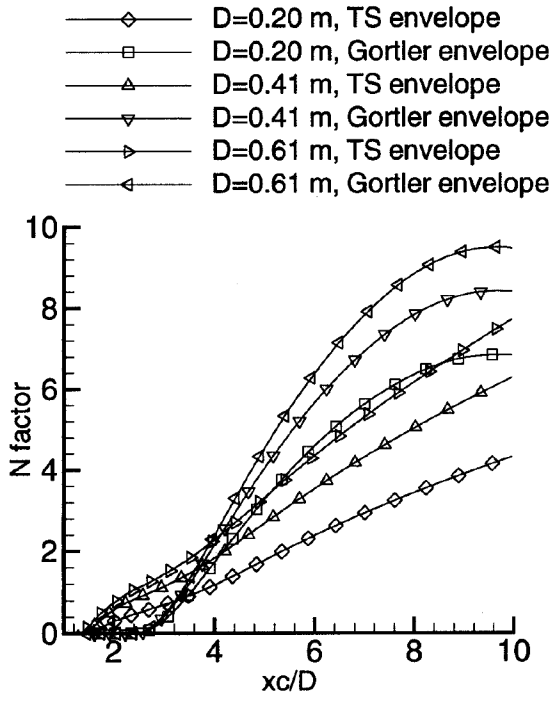

Figure 5. *N*-factor envelopes at three Reynolds numbers (g3, g5, g4, see Table 2).

Effect of Reynolds number

Figure 5 compares *N*-factors in the long Mach 6 nozzle, at three Reynolds numbers. As is true in general unless otherwise stated, the stagnation pressure is 1.03×10^6 Pa (150 psia) and the stagnation temperature is 456 K (820 R). Here, the wall temperature is isothermal, decreasing linearly with arclength from 456 K (820 R) at the bleed lip to 300 K (540 R) at the exit. The exit diameters are shown in the legend. Both TS (first mode) and Görtler rise with Reynolds number.

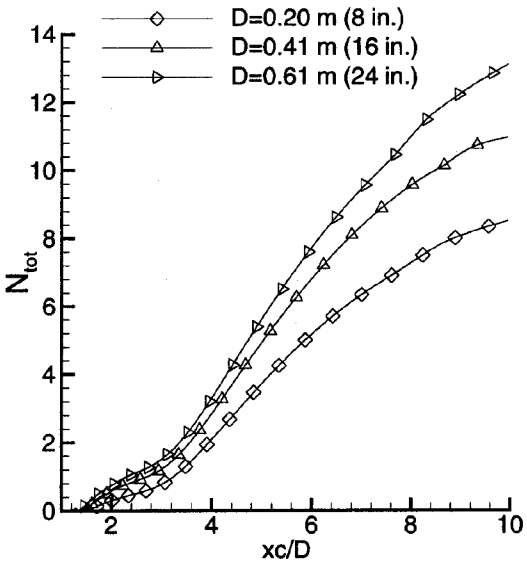

Figure 6. Total *N*-factors at three Reynolds numbers (g3, g5, g4, see Table 2).

Figure 6 shows the envelope of the three *N*-factors, including the second mode, and again taken with the square root of the sum of the squares. Using $N = 7.5$ the quiet Reynolds number was computed, with the results given in Table 2. The quiet Reynolds number increases with Reynolds number, but not as fast as it did for Chen's shorter nozzles. The performance of the long 0.20 m (8 in.) nozzle is about 50% better than the Langley 7.5 inch Mach 6; the performance of the 0.61 m (24 in.) is about 2 times better.

Effect of nozzle length at moderate Reynolds number

Figure 7 shows momentum thickness and Görtler number for the long and very long nozzles. Both nozzles also have isothermal wall temperatures that decrease linearly with arclength from 456 K (820 R) at the bleed lip tip to 300 K (540 R) at the exit, and both have 0.20 m (8 in.) exit diameters. Görtler number remains about the same as the nozzle is lengthened.

Figure 8 shows first-mode and Görtler envelopes for three 0.20 m (8 in.) nozzles. As started earlier m6chen6b has an adiabatic wall, while g3 and i1 have isothermal walls with a temperature that drops linearly with arclength from 456 K (820 R) to 300 K (540 R). The Görtler *N*-factors drop dramatically when the nozzle is

Table 2. Quiet Reynolds number vs Reynolds number for long nozzle

ID	Exit diam.	xc, $N = 6.5$	xc, $N = 7.5$	Re_{quiet}	D_q	L_q
g3	0.20 m	1.46 m	1.67 m	8.7 million	0.15 m	9.85 m
g5	0.41 m	2.39 m	2.61 m	9.7 million	0.16 m	0.98 m
g4	0.61 m	3.29 m	3.63 m	11.4 million	0.19 m	1.13 m

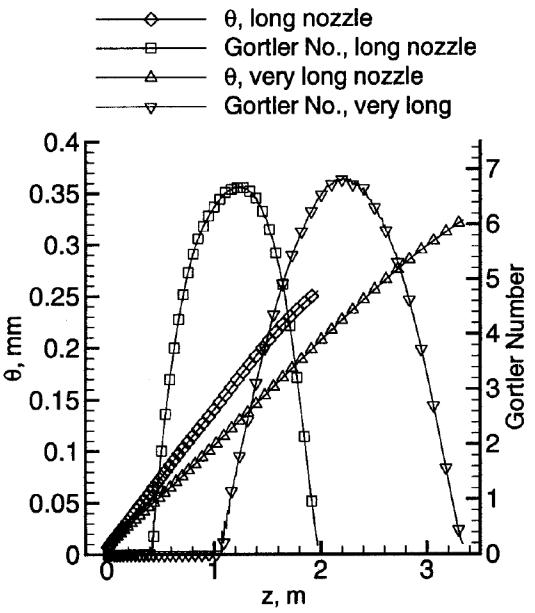

Figure 7. Momentum thickness and Görtler number in long and very long nozzles (g3, i1).

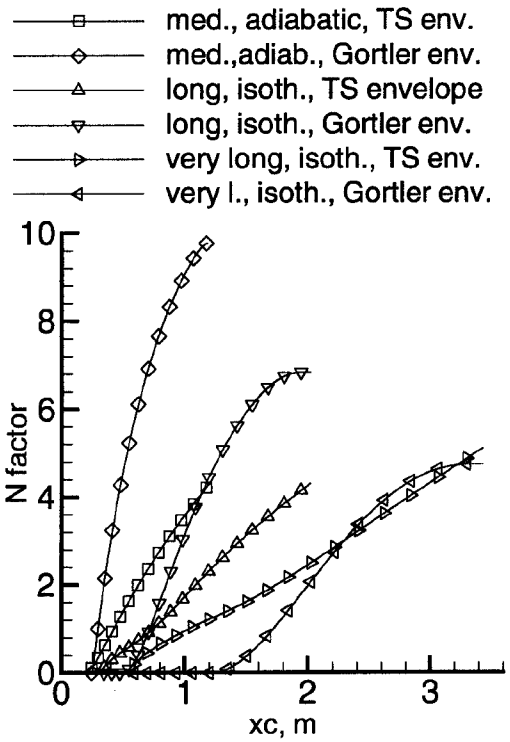

Figure 8. N-factor envelopes for three nozzle lengths (m6chen6b, g3, i1).

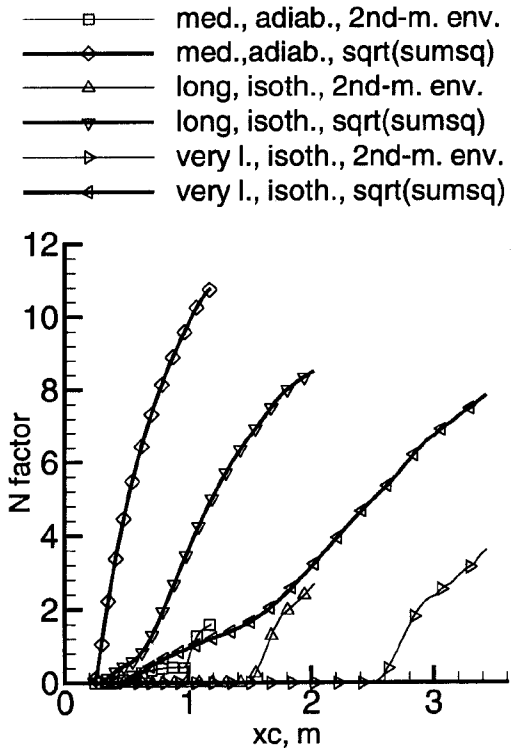

Figure 9. Total N-factors for three nozzles of different lengths (m6chen6b, g3, i1).

lengthened, but the first-mode increases with length for the two isothermal wall cases. Although peak Görtler number does not decrease when the nozzle is lengthened, Görtler N factors do decrease. The use of transition estimates based on the N-factors rather than the Görtler numbers is supported by previous Langley experience with lengthened nozzles[35].

Figure 9 shows the combined N-factors for the 3 nozzles, along with the second-mode envelopes. The long and very long nozzles have the same temperature distribution, the medium nozzle is similar to the Langley design and has the adiabatic wall temperature used at Langley. The key quiet-flow parameters are summarized in Table 3. The quiet Reynolds numbers increase with length because the first-mode instability increases less than the Görtler instability decreases.

Effect of length at high Reynolds number

Figure 10 shows the results for the very long nozzle when it is scaled up to increase the Reynolds number by

Table 3. Quiet Reynolds numbers vs nozzle length

ID	xc, $N = 6.5$	xc, $N = 7.5$	Re_{quiet}	D_q	L_q
m6chen6b	0.63 m	0.72 m	7.3 million	0.12 m	0.73 m
g3	1.46 m	1.67 m	8.7 million	0.15 m	0.85 m
i1	2.94 m	3.32 m	11.1 million	0.19 m	1.10 m

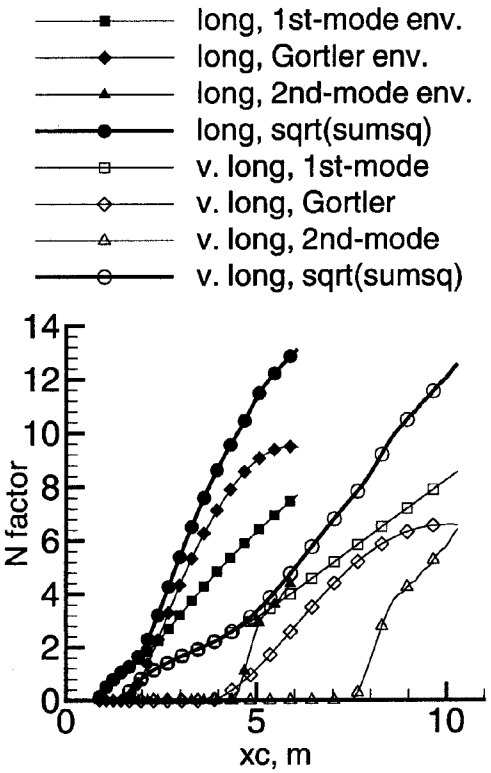

Figure 10. N-factors for long and very long nozzles at higher Reynolds number (g4, i2).

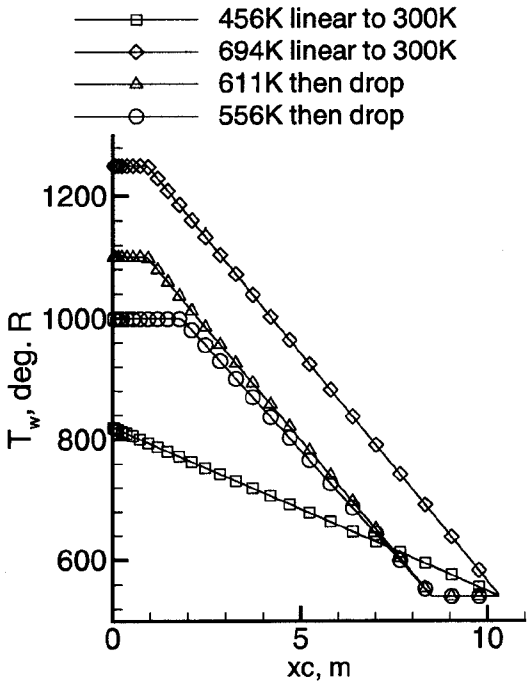

Figure 11. Various wall temperature distributions for very long nozzle (i2, i3, i4, i5).

a factor of 3. It is compared to the long nozzle at the same Reynolds number. Both nozzles now have 0.61 m (24 in.) inviscid exit diameters. Both nozzles have wall temperatures that taper linearly from 456 K (820 R) to 300 K (540 R). Every 10th point is shown. Using $N_{tot} = 7.5$ as a transition criterion, the very long nozzle has a quiet Reynolds number of 7.8 million, while the long nozzle has a quiet Reynolds number of 11.4 million.

The very long nozzle in the 0.61 m (24 in.) exit size has worse performance than it does in the 0.20 m (8 in.) exit size. It also has worse performance than the long 0.20 m (24 in.) nozzle does, although the very long 0.20 m (8 in.) is better than the long 0.20 m (8 in.). TS dominates the very long nozzle, whereas it is less than Görtler in the long nozzle. The combined N-factor is also shown. Although N_{tot} is lower at the nozzle exit for the very long nozzle, its performance is worse because $N = 7.5$ is reached farther upstream of the nozzle exit.

Although lengthening the nozzle works well at the moderate Reynolds number, the improvement is not sustained at the higher Reynolds number, due to increased problems with the first-mode instability. Another means of control is needed in order to reach high quiet Reynolds numbers.

Effect of nozzle wall temperature

It has already been shown that the temperature distribution at the nozzle wall is very important. A number of cases were then computed in order to see if the combined effect of wall temperature and nozzle length would allow reaching high quiet Reynolds numbers.

Figure 11 shows the temperature distributions for 4 such cases. All the nozzles have 0.61 m (24 in.) inviscid exit diameters. The first case, i2, begins with a wall temperature equal to the stagnation temperature, 456 K (820 R). It tapers linearly to nominal ambient temperature, 300 K (540 R), at the nozzle exit. This simulates a throat maintained at the driver-tube temperature of 456 K (820 R), and a nozzle exit cooled to maintain it at

Table 4. Quiet Reynolds number vs wall temperature for the very long 0.61 m (24 in.) nozzle

ID	xc, $N = 6.5$	xc, $N = 7.5$	Re_{quiet}	D_q	L_q
i2	6.86 m	7.44 m	7.8 million	0.13 m	0.76 m
i3	9.88 m	past exit	35.6 million	0.59 m	3.51 m
i4	9.11 m	past exit	35.6 million	0.59 m	3.51 m
i5	8.75 m	9.72 m	30.6 million	0.51 m	3.02 m

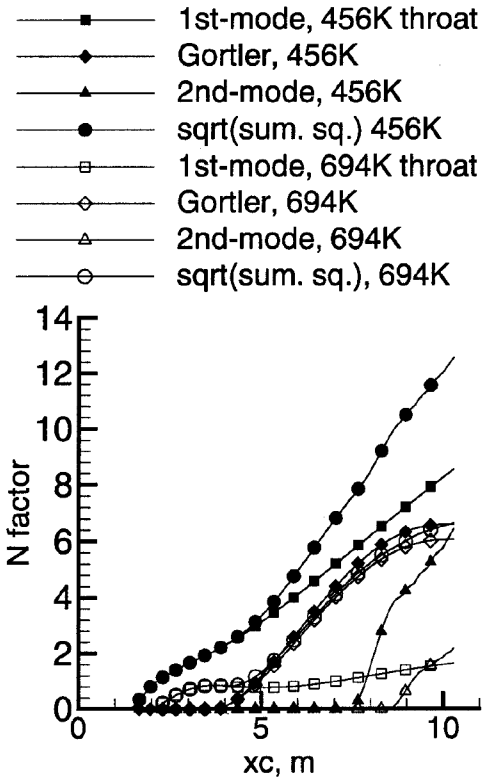

Figure 12. Effect of additional throat heating in very long nozzle (i2, i3).

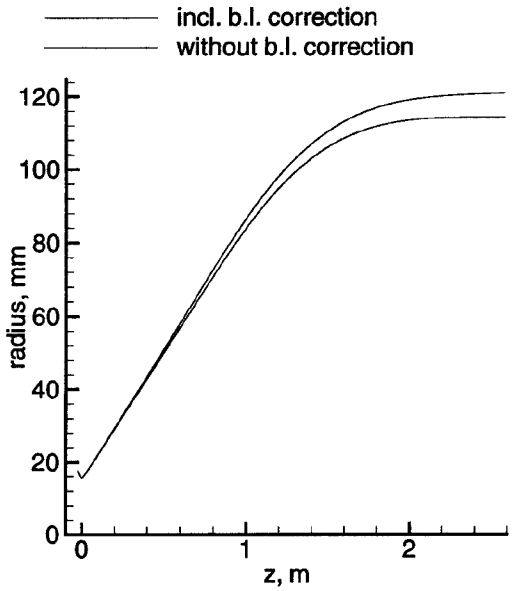

Figure 13. Contour for prototype nozzle (m1).

300 K (540 R), with a nominal constant-thermal-resistance path in between. The second case, i3, shows a throat maintained at 694 K (1250 R) over the first 0.91 m (3 ft) of arclength, followed by the same linear gradient down to ambient temperature at the exit. The third case, i4, is similar, except the throat is heated only to 611 K (1100 R), and the last 1.82 m (6 ft.) of the nozzle is held at room temperature. This simulates a case where the heat is taken out of the nozzle upstream of the last section where the windows are. The final case, i5, reduces the peak throat temperature further to 556 K (1000 R), but spreads it over a longer distance, 1.82 m (6 ft.), easing thermal-stress issues while maintaining a similar amount of total heat transfer into the boundary layer.

Figure 12 shows the dramatic effect of substantial heating at the throat. The envelopes of the most unstable waves are plotted for the nozzle, for each of the 3 types of instabilities, and for the square root of the sum of the squares. The Görtler instability is affected only weakly by the heating. The first-mode instability decreases dramatically, causing a dramatic decrease in N_{tot}.

Only the throat is heated, so the second-mode instability, which grows only near the exit, should not be affected much. Uniform heating decreases the growth of the second mode, so a decreasing wall temperature should make the wall look cold, increasing the second-mode growth. Unexpectedly, however, the second-mode waves decrease with the throat heating. This effect remains to be explained.

Throat heating is thus a very effective means of controlling the first-mode waves, and it also has a favourable effect on the second-mode waves. Table 4 summarizes the key results. For case i3 with the 694 K (1250 R) throat, N_{tot} does not reach 7.5 before the exit, where the computation halted. Transition is assumed at the nozzle exit, for a quiet Reynolds number in excess of 35.6 million. Quiet flow is predicted for a back-to-back cone with a half-length of 1.74 m (5.7 ft.) and a diameter of 0.58 m (1.9 ft.). This quiet-flow Reynolds number is sufficient to allow reproducing many flight experiments[44]. Lengthening the nozzle controls Görtler

Table 5. Quiet Reynolds number vs wall temperature for the prototype 0.23 m (9 in.) nozzle

ID	xc, $N = 6.5$	xc, $N = 7.5$	Re_{quiet}	D_q	L_q
m1	2.59 m	past exit	13.2 million	0.22 m	1.31 m
m2	1.98 m	2.26 m	10.2 million	0.17 m	1.01 m
m3	1.83 m	2.07 m	8.1 million	0.13 m	0.79 m

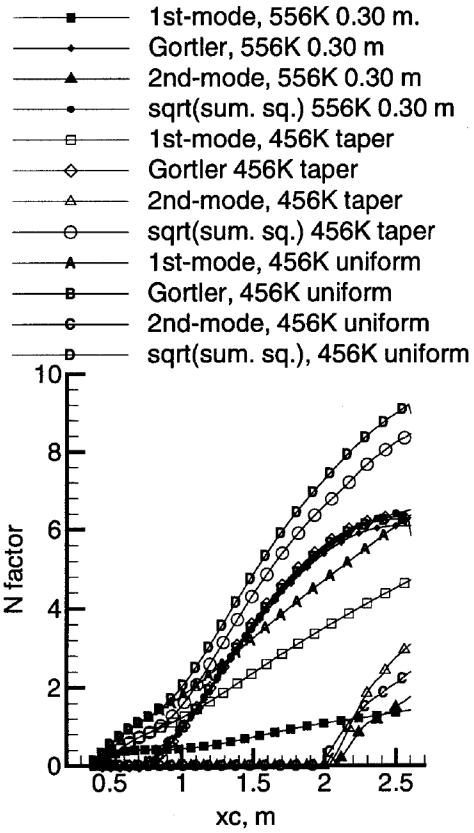

Figure 14. N-factor envelopes for prototype nozzle at three wall temperature distributions (m1, m2, m3).

instabilities, but causes problems with TS instabilities. However, when a long nozzle and a hot throat are combined, the result is a dramatic improvement.

Results at and near final design point for prototype

An inviscid exit diameter of 0.23 m (9.0 in.) was selected for the prototype. This diameter is a closer match to the inside diameter of commonly available thick-walled pipe, which can be used to fabricate some of the nozzle parts. It also should allow the use of the same models used in the open-jet 0.19 m (7.5 in.) nozzle at Langley. Since this prototype has an intermediate Reynolds number compared to the cases computed previously, further studies were carried out to determine an optimum length and the required throat temperatures. Detailed results are presented in ref. 34.

Figure 13 shows the contour of the final design for the prototype nozzle, which has a length of about 2.62 m (103 in.). Details of the inviscid contour are shown in Table 1. The relative length of the nozzle is less than that of the full-scale version because larger curvature is allowable at the lower Reynolds number. The correction due to displacement thickness is also shown in Figure 13; thickness is about 6 mm (1/4 in.) at the nozzle exit.

Figure 14 shows the N-factor envelopes in the prototype nozzle. Case m1 has a 556 K (1000 R) throat for the first 0.30 m (1 ft.) of arclength, followed by a linear taper to 300 K (540 R), where the last 0.61 m (2 ft.) is held. Case m2 has a linearly tapering isothermal temperature from 456 K (820 R) at the bleed lip tip to 300 K (540 R) at the exit. Case m3 has an isothermal wall that is 456 K (820 R) over the whole nozzle. Key parameters are shown in Table 5. The legend for the corresponding figure in ref. 34 is incorrect and has been corrected here. For the first case, which is the nominal design, N_{tot} never reaches 7.5. Transition is assumed at the nozzle exit, for the purpose of computing the numbers in the table.

The second and third cases with smaller throat temperatures have dramatically reduced performance. Clearly, some throat heating is essential to optimal operation of the nozzle, as is the requirement for the temperature to decrease with streamwise distance.

Summary

Using e^N methods, an 0.61 m (24 in.) Mach-6 nozzle is designed to remain quiet to a length Reynolds number in excess of 36 million. Lengthening the nozzle reduces the Görtler N factor, although it does not reduce the Görtler number. The nozzle-wall temperature is maintained above the stagnation temperature, near the throat, and is made to decrease to ambient near the exit. This temperature distribution greatly reduces the growth of first and second-mode instabilities. The reduction in the growth of the first mode was expected, but the reduction in the growth of the second mode remains to be explained. The two factors must be combined carefully to be effective.

An 0.23 m (9 in.) prototype is also designed, and should remain quiet to a length Reynolds number in excess of 13 million, according to similar e^N computations. This performance would be twice that of the best nozzle yet tested at hypersonic speeds. Construction of

the prototype is well underway, and should be completed late in 2000.

Nomenclature

D exit diameter of inviscid nozzle
D_q diameter of the quiet uniform region
G Görtler number, $G = (U\theta/\nu)\sqrt{\theta/R}$
L_q length of the quiet uniform region, from tip to tip
N_{tot} square root of sum of squares of N factors for individual instabilities
P_t total or stagnation pressure
R concave-wall radius of curvature
R_∞ unit Reynolds number in nozzle freestream
$R_{\Delta x}$ Reynolds number based on R_∞ and Δx
RC radius of curvature at the nozzle throat, throat radii
T_t total or stagnation temperature
T_w wall temperature
U velocity at the boundary layer edge
x_a axial location of the end of radial flow at the nozzle wall, throat radii
x_d axial location of the nozzle exit, throat radii
x_g axial location of the beginning of radial flow at the nozzle wall, throat radii
xc arclength along the nozzle wall from the bleed lip tip
y_a radial location of the end of radial flow at the nozzle wall, throat radii
y_d radial location of the inviscid nozzle exit, throat radii
y_g radial location of the beginning of radial flow at the nozzle wall, throat radii
z axial coordinate down nozzle centerline, origin at throat
θ momentum thickness
Δx axial length of uniform and quiet nozzle flow
ν kinematic visocity at the boundary layer edge
η wall angle at the inflection point, degrees

1. Berry, S. A., Horvath, T. J., Hollis, B. R., Thompson, R. A. and Hamilton II, H. H., X-33 hypersonic boundary layer transition, *AIAA*, Paper 99–3560, June 1999.
2. Korejwo, H. A. and Holden, M. S., *AIAA*, paper 92–1074, February 1992.
3. AGARD, *Sustained Hypersonic Flight*, April 1997, CP-600, vol. 3.
4. Bushnell, D. M., in *Instability and Transition* (eds Hussaini, M. Y. and Voigt, R. G.), Springer-Verlag, New York, 1990, Paper 217–232, Materials of the workshop held May 15 – June 9 1989 in Hampton, Virginia.
5. Reshotko, E., *AIAA*, 1994, Paper 94–0001, The 1994 Dryden Lecture in Research.
6. Floryan, J. M., *Prog. Aerospace Sci.*, 1991, **28**, 235–271.
7. Mack, L. M., in *Report 709, Special Course on Stability and Transition of Laminar Flow*, AGARD, 1984, pp. 1–81.
8. Reed, H. L. and Saric, W. S., *Annu. Rev. Fluid Mech.*, 1989, **21**, 235–284.
9. Herbert, Th., *Annu. Rev. Fluid Mech.*, 1988, **20**, 487–526.
10. Narasimha, R., *Prog. Aerospace Sci.*, 1985, **22**, 29–80.
11. Malik, M. R., *AIAA J.*, 1989, **27**, 1487–1493.
12. Reed, H., Kimmel, R., Arnal, D. and Schneider, S., in *Sustained Hypersonic Flight*, AGARD, April 1997. Paper C15 in *CP-600*, vol. 3, Also appears as AIAA Paper 97-1818, 1997.
13. Beckwith, I. E. and Miller III, C. G., *Annu. Rev. Fluid Mech.*, 1990, **22**, 419–439.
14. Wilkinson, S. P., Anders, S. G. and Chen, F.-J., *AIAA*, 1994, paper 94–2498.
15. Chen, F.-J., Malik, M. R. and Beckwith, I. E., *AIAA J.*, 1989, **27**, 687–693.
16. Blanchard, A. E., Lachowicz, J. T. and Wilkinson, S. P., *AIAA J.*, 1997, **35**, 23–28.
17. Wilkinson, S., *AIAA*, paper 97-1819, June 1997.
18. Schneider, S. P., in *Laminar-Turbulent Transition: Proceedings of the 1999 IUTAM Conference, Sedona*, Springer-Verlag, New York, 2000, to appear.
19. Schneider, S. P., *AIAA*, 2000, paper 2000-0295.
20. Stetson, K. F. and Kimmel, R. L., *AIAA J.*, 1992, **30**, 2974–2976.
21. Braslow, A. L., TN D-3384, NASA, August 1966.
22. Chen, F. J., Wilkinson, S. P. and Beckwith, I. E., *J. Spacecraft Rockets*, 1993, **30**, 170–175.
23. Sivells, J. C., Technical Report AEDC-TR-78-63, Arnold Engineering Development Center, USA, December 1978.
24. Sivells, J. C., *J. Spacecraft*, 1970, **7**, 1292–1299.
25. Nelms, L. T., Technical Report AEDC-TR-68-212, Arnold Engineering Development Center, USA, 1968.
26. Harris, J. E. and Blanchard, D. K., Technical Report NASA-TM-83207, NASA, February 1982.
27. Malik, M. R., *J. Comput. Phys.*, 1990, **86**, 376–413.
28. Malik, M. R., Technical Report HTC-8902, High Technology Corporation, Hampton, VA, March 1989. See also HTC-9203, which is almost identical.
29. Schneider, S. P., Contractor Report CR-197286, NASA, January 1995.
30. Alcenius, T. and Schneider, S. P., Contractor Report CR-194857, NASA, January 1994.
31. Alcenius, T., Schneider, S. P., Beckwith, I. E. and Korte, J. J., *AIAA*, June 1994, Paper 94-2578.
32. Schneider, S. P., *AIAA*, June 1988, paper 98-2511.
33. Kufner, E., Dallman, U. and Stilla, J., *AIAA*, July 1993, Paper 93-2983.
34. Schneider, S. P., *AIAA*, January 1998, Paper 98-0547.
35. Chen, F.-J., Malik, M. R. and Beckwith, I. E., *AIAA J.*, 1992, **30**, 2093–2094.
36. Chen, F. J. and Wilkinson, S. P., *AIAA*, June 1994, Paper 94-2506.
37. Demetriades, A., *AIAA J.*, 1996, **34**, 2490–2495.
38. Masad, J. A. and Nayfeh, A. H., *Phys. Fluids A*, 1992, **4**, 1259–1272.
39. Harvey, W. D., Stainback, P. C., Anders, J. B. and Cary, A. M., *AIAA J.*, 1975, **13**, 307–314.
40. Schneider, S. P. and Munro, S. E., *AIAA J.*, 1998, **36**, 872–873.
41. Lin, R.-S., Iyer, V. and Malik, M. R., *AIAA*, 1998, Paper 98-2437.
42. Chen, F. J., Wilkinson, S. P. and Beckwith, I. E., *AIAA*, 1991, Paper 91-1648.
43. Schrauf, G., Bieler, H. and Thiede, P., in Proceedings of the First European Forum on Laminar Flow Technology, Hamburg, 1992, pp. 73–82.
44. Schneider, S. P., *J. Spacecraft Rockets*, 1999, **36**, 1–13.

ACKNOWLEDGEMENTS. This design work was funded by the US AFOSR under grant F49620-97-1-0037, originally monitored by Len Sakell and now monitored by Steve Walker. The generous cooperation of the NASA Langley quiet tunnel group is appreciated. Matching funds for tunnel construction are provided by a gift from the Boeing Company.